Physics-based image enhancement for infrared thermography

Stephen D. Holland*,[a], Jeremy Renshaw[b]

[a] *Department of Aerospace Engineering and Center for Nondestructive Evaluation*
Iowa State University
1915 Scholl Road
Ames, IA 50011
[b] *Department of Materials Science and Engineering and Center for Nondestructive Evaluation*
Iowa State University
Ames, IA 50011

Abstract

Thermal imaging with an infrared camera can be used to view the location and intensity of heat sources in space and time. In a thermal conductor, thermal diffusion blurs out those heat sources. Knowledge of the physics of thermal diffusion can be used to enhance the spatial and temporal resolution of thermal images. In two dimensions, quantitative reconstruction of the heat source intensity is possible. The same algorithm applied to three-dimensional heat flows provides dramatic improvements in temporal and spatial resolution of the thermal images. Performance is illustrated both in theory and by experiment. An application example demonstrates utility to nondestructive evaluation.

Key words: Flash Thermography, Vibrothermography, Sonic Infrared, Sonic IR, image processing, image enhancement, Laplacian filter

DOI: `http://dx.doi.org/10.1016/j.ndteint.2010.04.004`

*Corresponding author
Email addresses: `sdh4@iastate.edu` (Stephen D. Holland), `renshaw@iastate.edu` (Jeremy Renshaw)

1. Introduction

Thermographic Nondestructive Evaluation (NDE) finds flaws or determines material properties through infrared measurement of heat patterns or temperature changes. Modern infrared thermography uses real-time video/digital imaging through semiconductor focal plane arrays or microbolometer arrays[1]. Given a blackbody – an object with perfect surface infrared emissivity – a thermal imaging camera can take accurate remote temperature measurements. Flash thermography involves excitation of a surface with a flash (impulse) of thermal energy, then monitoring surface cooling or thermal transmission [2]. Established algorithms [3] can be used to measure thickness or identify delaminations in composite materials. Spatial resolution enhancement through methods such as inverse scattering [4] have been in use for many years to enhance the resolution of flash thermography images. Vibrothermography, also known as "thermosonics" and "sonic infrared", is an emerging inspection technology that finds cracks and delaminations by observing heat generated from frictional rubbing of vibrating crack surfaces [5]. Typically a high power sonic or ultrasonic transducer vibrates the specimen for approximately one second. The heating of the crack and the diffusion of the heat are observed with the infrared camera.

For the most part, infrared images are treated and processed similarly to visible light images. Standard denoising and sharpening algorithms are commonly used with infrared images[1], although these algorithms were originally intended to compensate for optical blurring, not the thermal diffusion prevalent in infrared images. There are also common processing and analysis steps that have been modified specifically for thermal images [6], including contrast evaluation, wavelet analysis, and principal component analysis. The quantitative nature of the infrared image combined with the known physics of heat conduction create the opportunity to develop processing algorithms that operate on physically meaningful quantities and take advantage of knowledge of heat conduction. In flash thermography, algorithms based primarily on one-dimensional heat diffusion [3] are often used to enhance image quality and estimate flaw depths.

There are various methods and algorithms discussed in the literature for inversion of thermal data. In general, inversion of thermal diffusion is ill-posed because of the diffusive nature of heat conduction. Inversion techniques for flash thermography attempt to estimate thickness from the conduction-driven cool-down profile of a surface exposed to a thermal impulse. The

approach of Shepard et al. [3] uses the time when 1D thermal diffusion slows, estimated from the inflection point of a log temperature vs. log time graph, to estimate thickness. The present work focuses on a different problem: Enhancement of lateral resolution of a surface or buried heat source. Several authors have reported analyses of flash thermography data using 3D heat-diffusion simulation [7, 8, 9] to improve resolution. Le Niliot [10] reports on a boundary element-based method for identifying the time-dependence of line heat sources when their position is known. Rainiere and Pagliarini [11] report on a Wiener filter-based method for determining the spatial distribution of the thermal diffusivity α. Spatial deconvolution of point spread functions is an established method [12],[13] to improve the resolution of thermal images of subsurface sources.

In this paper, we report on a simple but effective algorithm based on the heat conduction equation for enhancement and analysis of infrared thermal images. While our method determines the heat source intensity, it does so by observation rather than inversion of the heat diffusion process. As such, it avoids the inherent difficulties in inverting diffusion.

2. Theory

Heat conduction in a solid is governed by the heat conduction (diffusion) equation,

$$\frac{\partial^2 T}{\partial x^2} + \frac{\partial^2 T}{\partial y^2} + \frac{\partial^2 T}{\partial z^2} + \frac{1}{k} g(x, y, z, t) = \frac{1}{\alpha} \frac{\partial T}{\partial t} \tag{1}$$

where T is temperature, k is thermal conductivity, $g(x, y, z, t)$ is the volumetric heat source distribution, and α is the thermal diffusivity [14].

Consider the two-dimensional case of a thin sheet or plate. The heat conduction equation reduces to

$$\frac{\partial^2 T}{\partial x^2} + \frac{\partial^2 T}{\partial y^2} + \frac{1}{k} g(x, y, t) = \frac{1}{\alpha} \frac{\partial T}{\partial t}. \tag{2}$$

At the surface of a specimen, the spatial (x, y) and temporal temperature distribution can be recorded with an infrared camera. The partial derivatives can be directly measured from such a sequence of calibrated infrared images of the surface of the sheet or plate. Given known or estimated thermal conductivity k, diffusivity α, and a measured sequence of infrared images,

the heat source distribution $g(x, y, t)$ can be measured by solving Eq. 2,

$$g(x, y, t) = \frac{k}{\alpha}\frac{\partial T}{\partial t} - k\left(\frac{\partial^2 T}{\partial x^2} + \frac{\partial^2 T}{\partial y^2}\right), \tag{3}$$

where k/α is equivalent to the density ρ times the specific heat c_P.

Eq. 3 provides a means to evaluate the spatial and temporal heat source distribution of a two-dimensional sheet or plate from infrared images of the surface temperature. In the time-independent case ($\partial T/\partial t = 0$), this is essentially a Laplacian method [15],[16]. Eq. 3 uses the known thermal conduction properties of the sheet or plate to subtract out diffusion effects. Only the heat source intensity $g(x, y, t)$, measured in Watts/meter^3, remains. Equation 3 is an exact solution that allows quantitative measurement of the two-dimensional heat source intensity from infrared images, and offers the potential to dramatically increase the resolution of thermal images by eliminating the blurring effect of thermal diffusion.

Unfortunately no similar solution exists for heat sources in a three-dimensional solid. An infrared camera can only measure surface temperatures and thus the depth diffusion term, $\partial^2 T/\partial z^2$ in Eq. 1 is not measurable. Equation 3 can still be applied to the surface, but it is no longer exact nor physically quantitative. Nevertheless, both theory and experiment demonstrate that Eq. 3 can provide dramatic improvements in the spatial and temporal resolution of thermal images even when heat flows are three dimensional. We will call the result of applying Eq. 3 to a surface image of heat flow in a three-dimensional solid the *heat source estimate* $\tilde{g}(x, y, t)$.

To predict the characteristics of Eq. 3 in a three-dimensional solid, we start with the well-known Green's function solution [17], and apply the method of images to determine the temperature field of a point impulse heat source at depth z_s below a free surface at $(x_s, y_s) = (0, 0)$ and $t_s = 0$,

$$T(x, y, z, t) = \frac{1}{(4\pi\alpha t)^{3/2}}\left[\exp\left(-\frac{x^2 + y^2 + (z - z_s)^2}{4\alpha t}\right) + \exp\left(-\frac{x^2 + y^2 + (z + z_s)^2}{4\alpha t}\right)\right] u(t), \tag{4}$$

where $u(t)$ represents the Heaviside unit step. Eq. 4 is the Green's function (impulse response) for thermal conduction of an impulse heat source at a distance z_s below the free surface $z = 0$.

By applying Eq. 3 to the Green's function temperature distribution, Eq. 4, we can evaluate the performance of the heat source estimate evaluated from Eq. 3 in eliminating the spatial and temporal spreading caused by thermal

diffusion. Substitution of Eq. 4 into Eq. 3 at the $z = 0$ free surface (via Eq. 1 and the second spatial derivative of Eq. 4) yields the heat source estimate $\tilde{g}(x, y, t)$ for an impulse source,

$$\tilde{g}(x, y, z = 0, t) = k \frac{\partial^2 T}{\partial z^2}\bigg|_{z=0} = \frac{k}{2\alpha t}\left(\frac{z_s^2}{2\alpha t} - 1\right) T u(t), \tag{5}$$

where T references the Green's function temperature distribution (Eq. 4) for a heat source a distance z_s below the surface. In summary, the source distribution $\tilde{g}(x, y, t)$ of Eq. 5 is equivalent to the processed image sequence resulting from applying Eq. 3 to images of the temperature field of a subsurface impulse heat source at $t = 0$ and $(x, y) = (0, 0)$. The fundamental characteristic of processing 3D data with Eq. 3 is immediately apparent from Eq. 5: The thermal response is dramatically attenuated with time. At short times $t << z_s^2/2\alpha$ after the impulse, the thermal response is attenuated with $1/t^2$. At later times $t >> z_s^2/2\alpha$, it is attenuated with $1/t$ in the heat source estimate.

Figure 1 shows the improvement in time resolution achieved in the heat source estimate $\tilde{g}$ compared with raw thermal images. It shows temporal impulse response curves at different in-plane source distances $r = \sqrt{x^2 + y^2}$ for both the thermal Green's function (Eq.4, solid) and the processed equivalent (Eq. 5, dashed). The impulse response for a processed sequence peaks more than twice as fast as an unprocessed sequence, and drops off much faster too! In parallel the amplitude of a processed sequence also drops off faster with source distance than in the unprocessed sequence.

Figure 2 provides a quantitative view of the improvement in time resolution. Fig. 2a shows that the peak of the impulse response will arrive at least 40% earlier in the processed image sequence than in the unprocessed sequence. Likewise, Figure 2b shows that the impulse response for a processed sequence decays at least seven times faster than an unprocessed sequence. The far faster response and decay of the processed image confirms that the processing algorithm dramatically enhances the temporal resolution of the thermal image sequence.

The breadth of blurring due to thermal diffusion increases with time. The Green's function, Eq. 4, can be thought of as a Gaussian of width $4\alpha t$. Therefore the increased time resolution causes a corresponding improvement in spatial resolution. One example of the increased spatial resolution can be found in the equilibrium heat distribution of a constant power heat source

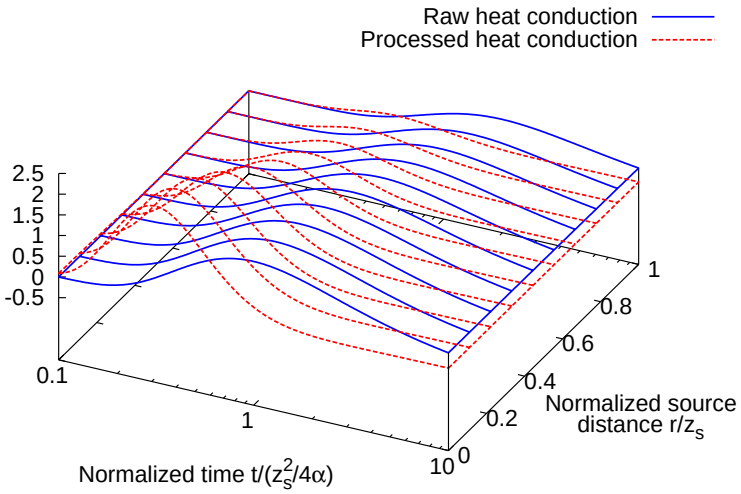

Figure 1: Calculated temporal impulse response curves for thermal diffusion of an impulse before (solid, Eq. 4) and after (dashed, Eq. 5) processing at different in-plane source distances $r = \sqrt{x^2 + y^2}$. Plotted logarithmically along the time axis so that the curves can be compared despite the far slower response in the raw data. (color online)

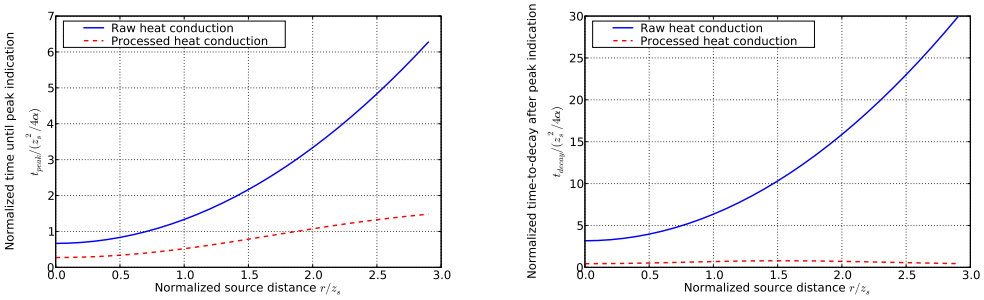

(a) (b)

Figure 2: (a) Time required for the raw or processed thermal image of the response to a thermal impulse to reach its maximum, as calculated from Eqs. 4 and 5. (b) Time required for the maximum to decay to 25% of its peak value, as calculated from Eqs. 4 and 5. Smaller values represent better temporal resolution. (color online)

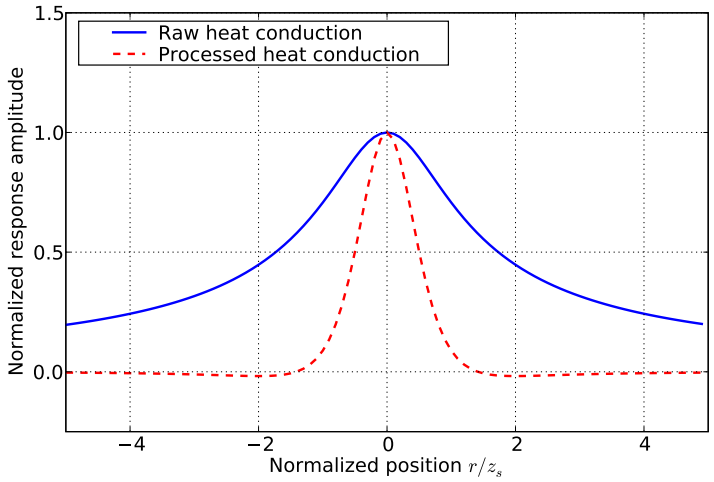

Figure 3: Calculated raw equilibrium temperature profile of a buried point heat source due to thermal diffusion (Eq. 6) and processed/enhanced profile (Eq. 7). (color online)

embedded in an infinite half-space thermal conductor. Counterintuitively, the equilibrium temperature state is finite (the apparent paradox of infinite energy delivery and finite temperature is resolved by the infinite size of the thermal conductor). The equilibrium temperature distribution is readily calculated from the time integral of the Green's function,

$$\int_{t=0}^{\infty} T(x,y,z=0,t)dt = \frac{1}{2\pi\alpha\sqrt{x^2+y^2+z_s^2}}. \tag{6}$$

When the temperature distribution reaches an equilibrium, the result of processing it with Eq. 3 also reaches equilibrium. This is readily calculated from the integral of Eq. 5 or by application of Eq. 3 to Eq. 6,

$$\int_{t=0}^{\infty} g(x,y,t)dt = \frac{k}{2\alpha\pi(x^2+y^2+z_s^2)^{3/2}}\left(\frac{3z_s^2}{x^2+y^2+z_s^2}-1\right). \tag{7}$$

Figure 3 shows a spatial profile of the equilibrium temperature distribution from a point subsurface heat source represented as a solid line as calculated from Eq. 6. The dashed line in Fig. 3 represents the profile of the same heat source after processing/enhancement, as calculated from Eq. 7.

Figure 3 shows that the processed image will have 3.5 times the resolution (width reduced by factor of 3.5) at the half maximum point and 5.2 times the resolution (width reduced by factor of 5.2) at the quarter-maximum point. Processing with Eq. 3 causes substantial improvements in spatial resolution as well as time resolution.

The proposed algorithm is not without drawbacks. The first- and second-order derivatives in Eq. 3 can cause dramatic noise gain. Low-pass spatial and/or temporal filtering is needed to avoid excessive noise levels, and the impulse response of the filter limits the ultimate resolution of the enhanced image sequence. In some cases, such as vibrothermographic tests where the heating is known to occur over a particular time window and only spatial resolution is desired, much of the noise can be eliminated through integration over the time window. The noise gain could also be dramatically reduced by curve-fitting the time-response of each pixel, as is commonly done for flash thermography [3]. Another possible disadvantage of the proposed algorithm is reduced sensitivity to deep heat sources compared with near-surface sources. Steady state thermal response to a buried source drops off with $1/z_s$ (Eq. 6) whereas the steady state response in the enhanced image drops off with $1/z_s^3$ (Eq. 7).

3. Experiment

To demonstrate the application of Eq. 3 to experimental data, we first illustrate the two-dimensional (exact) case. We heated the back side of an IR-opaque thin (0.5 mm) sheet of black-painted steel using an overhead projector. A (negative) stencil in an irregular staircase pattern on the projector provides a 100 mm wide shape. The front side of the steel sheet was imaged with a thermal infrared camera, revealing the pattern. In this case $g(x, y, t)$ represents the thermal energy delivered by the projector less radiative and convective losses. A series of infrared images of the surface temperature were recorded as the sheet was heated and began to cool. The image sequence was processed according to Eq. 3 plus low-pass spatial filtering to limit noise gain. Figure 4 shows snapshots from the unprocessed and processed sequences of infrared images of the front side of the sheet. The upper row shows raw thermal images as the sheet is heated from behind by the projector at t=2, 5, and 16 seconds, and at t=24 seconds after the projector has been turned off. The middle row shows the processed thermal images from the same times. As the surface heats up the raw thermal image is observed to bloom and

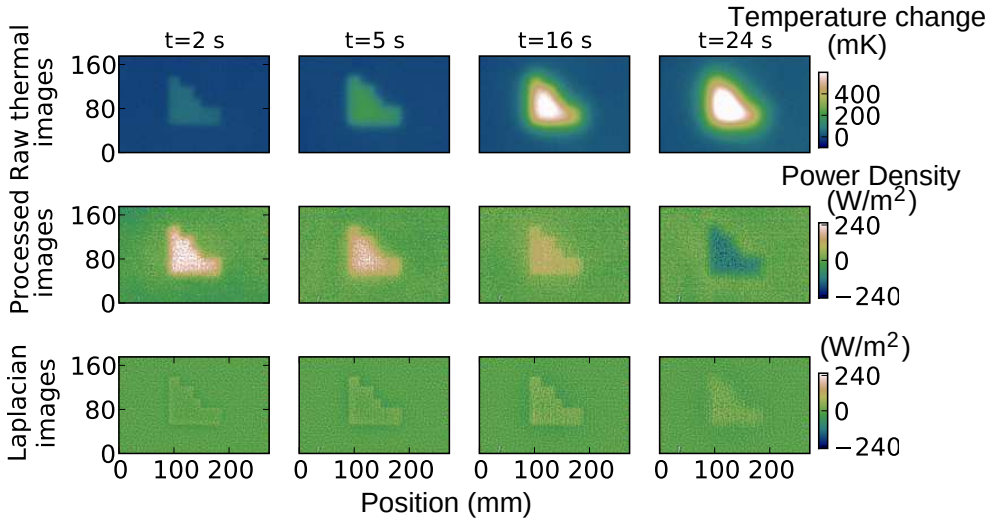

Figure 4: Unprocessed and processed (Eq. 3, divided by thickness to give Watts/m^2) images of 2D heat flow. The heat source was turned on at t=0 s and off at t=23 s, between the third and fourth frames. The fourth processed frame shows negative contrast due to convective and radiative cooling. Laplacian images (Eq. 3 with the time-derivative term removed) are included in the third row for comparison purposes. (Color online)

blur due to thermal diffusion, with temperature changes exceeding 500mK. There is no clear indication in the last frame of the raw images that the heat source has been turned off and the surface is cooling. The processed images of $g(x, y, t)$ in the middle row show net heat delivery that starts at around 240 W/cm^2 but then falls to around 160 W/cm^2 as convective and radiative losses increase. The convective and radiative heat loss continues at around -120 W/cm^2 after the source is turned off (negative contrast). The processed images show the characteristic shape of the stencil with similar resolution at all time steps, in contrast with the increasing blurriness of the raw images. From these data combined with the extremely simple and well established theory of Eqs 2 and 3 we conclude that Eq. 3 can be used to evaluate the spatial heat source distribution in two dimensions. For purposes of comparison, the Laplacian terms alone $-k\left(\frac{\partial^2 T}{\partial x^2} + \frac{\partial^2 T}{\partial y^2}\right)$ were calculated separately and plotted with the same scale in the bottom row. The Laplacian terms, while having similar or possibly slightly sharper resolution do not have the same physical meaning as in Eq. 3. For example at t=24 seconds in Fig. 4 the Laplacian still shows a positive image, where in reality the surface is cooling, as represented in the middle row processed with Eq. 3.

In a three dimensional medium, Eq. 3 is no longer exact. It no longer provides a means to quantitatively evaluate heat flow. Nevertheless, from Eqs. 5 and 7 as represented in Figs. 1-3, dramatic resolution enhancement is still possible. To evaluate the resolution enhancement, step and pulse heat sources were applied below the surface of a steel specimen. In each case the surface temperature was imaged using an infrared camera and processed using Eq. 3 plus spatial low pass filtering.

Figure 5 shows unprocessed and processed thermal infrared images of surface temperature of the steel specimen caused by a two-second ($t = -1..1$s) heat pulse, intended as an approximation of an impulse at $t = 0$. The pulse was generated by the tip of a 260 Watt soldering gun, 21 mm below the surface. The tip was embedded in a hole from the opposite side and surrounded with solder to couple nearly all the energy to the surrounding steel. Fig. 5 also shows expected profiles calculated from Eqs. 4 and 5 for an impulse source at that depth[1]. Temporal resolution is dramatically better in

[1]Since there was no independent measure of the thermal diffusivity α available for this specimen, α was adjusted as a free parameter to match the observed diffusion and this value of α was used in processing Figs. 5 and 6.

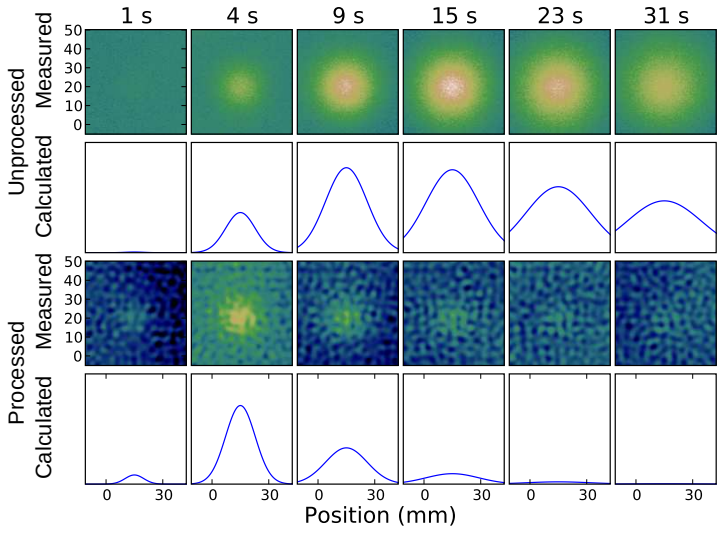

Figure 5: Unprocessed and processed thermal infrared images of surface temperature caused by a pulse from a buried heat source. Calculated profiles, from Eqs. 4 and 5, are included for comparison. (Color online)

the processed images than the unprocessed images, with substantial decay by the third frame at $t = 9$s, whereas the unprocessed images show significant decay only in the last frame of Fig. 5 at $t = 31$s. Spatial resolution is also improved through rejection of the broad, diffused heat profiles at $t = 9$s and beyond. Figure 6 shows thermal images from a stepped heat source, a 25W soldering iron tip, 6 mm below the surface. The thermal response approaches its equilibrium distribution, as seen in the top row of frames. The processed heat source estimate, shown in the bottom row of frames, approaches its equilibrium much more rapidly. In addition, the processed equilibrium distribution is much sharper than the unprocessed distribution. Figures 4-6 show that application of Eq. 3 can, in practice as well as theory, provide dramatic improvements in temporal and spatial resolution of thermal images.

The processing algorithm, Eq. 3, has real and significant application in the field of thermal nondestructive evaluation. A recently developed method for evaluating crack closure stress profiles based on the loci of frictional rubbing [18] becomes much more effective when the resolution of the thermal image is increased. While the physical scale is an order of magnitude smaller in size

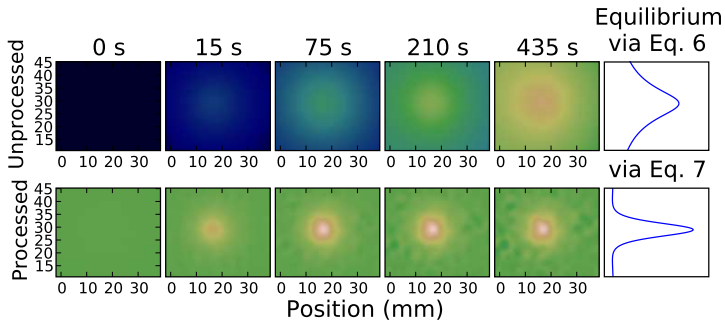

Figure 6: Unprocessed and processed thermal infrared images of surface temperature caused by a a stepped buried heat source. Calculated equilibrium profiles, from Eqs. 6 and 7, are included for comparison. (Color online.)

(cm to mm) and three orders of magnitude smaller in energy, the physics is the same. Figure 7 shows the dramatic resolution enhancement of a thermal image of vibration-induced frictional crack heating achieved through application of Eq. 3. The image on the left is a snapshot of a single unprocessed frame. The image on the right is the processed image, integrated (averaged) over all the frames during the vibrational excitation. The finer spatial resolution provided by the processing allows more precise identification of heat loci, which indicate regions of the crack under low but non-zero closure stress and which are used to evaluate the crack's closure stress profile. The noise gain caused by Eq. 3 is largely mitigated through integration over the time window when the vibration was occurring.

4. Conclusions

Heat source intensity estimation using Eq. 3 provides a means to improve the temporal and spatial resolution of thermal images recorded using an infrared camera. For two-dimensional heat flow the analysis is (in theory) exact and quantitative. With three-dimensional heat flow, Eq. 3 dramatically improves the qualitative localization of heat sources in space and time, and its benefits have been illustrated both in theory and by experiment. Application of Eq. 3 increases noise levels. This noise gain can be partially mitigated by low-pass spatial or temporal filtering, as well as integration (averaging) over a known pulse width. The algorithm is useful and relevant in the fields of infrared thermography and nondestructive evaluation.

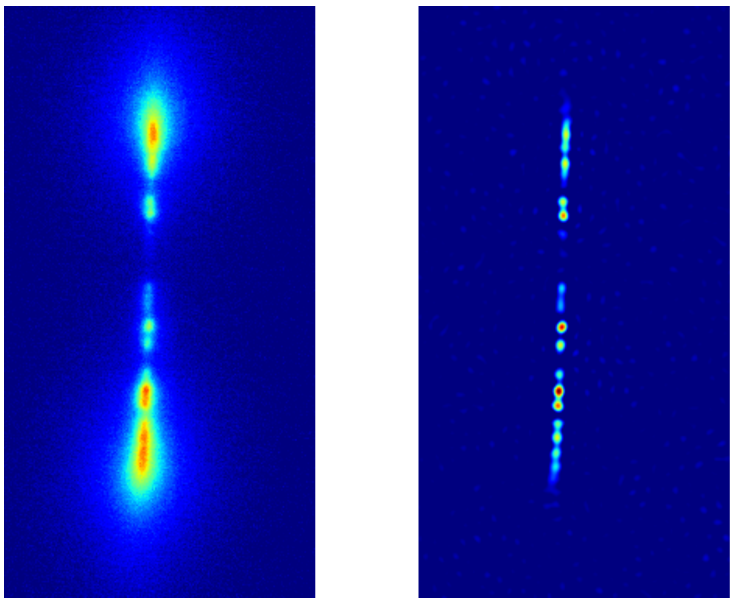

Figure 7: Raw (left) and processed (right) images of vibration induced frictional heating of a crack in titanium. (Color online)

5. Acknowledgements

This material is based upon work supported by the Air Force Research Laboratory under Contract #FA8650-04-C-5228 at Iowa State University's Center for NDE.

References

[1] X. Maldague, *Theory and Practice of Infrared Technology for Nondestructive Testing* , John Wiley and Sons, New York (2001).

[2] J. M. Milne and W. N. Reynolds, "The non-destructive evaluation of composites and other materials by thermal pulse video thermography", Thermosense VII in Proc. SPIE **520** 119 (1985)

[3] S. M. Shepard, J. R. Lhota, B. A. Rubadeux, D. Wang, and T. Ahmed, "Reconstruction and enhancement of active thermographic image sequences", Opt. Eng. **42**(5) 1337-1342 (2003)

[4] D. J. Crowther, L. D. Favro, P. K. Kuo, and R. L. Thomas, "Inverse scattering algorithm applied to infrared thermal wave images", J. Appl. Phys. **74**(9) 5828-5834 (1993)

[5] M. Morbidini, P. Cawley, T. Barden, D. Almond, and P. Duffour, "Prediction of the thermosonic signal from fatigue cracks in metals using vibration damping measurements", J. Appl. Phys. **100**, 104905 (2006)

[6] C. Ibarra-Castanedo, D. González, M. Klein, M. Pilla, S. Vallerand, and X. Maldague, "Infrared image processing and data analysis", Infrared Phys. & Tech. **46** 75-83 (2004)

[7] T. S. Durrani, A. Rauf, K. Boyle, F. Lotti, and S. Baronti, "Thermal imaging techniques for the non destructive inspection of composite materials in real time", Proc. IEEE Intern. Conf. on Acoust., Speech, and Signal Processing **12** 598-601 (1987)

[8] U. Seidel, K. Haupt, H. G. Walther, J. A. Burt, and M. Munidasa, "An attempt towards quantitative photothermal microscopy", J. Appl. Phys **78**(3) 2050-2056 (1995)

[9] E. Grinzato and V. Vavilov, "Corrosion evaluation by thermal image processing and 3D modelling", Rev. Gen. Therm. **37** 669-679, 1998

[10] C. Le Niliot, "The boundary-element method for the time-varying strength estimation of point heat sources: application to a two-dimensional diffusion system", Numerical Heat Transfer, Part B, **33** 301-321 (1998)

[11] S. Rainieri and G. Pagliarini, Data filtering applied to infrared thermographic measurements intended for the estimation of local heat transfer coefficient, Experimental Thermal and Fluid Science **26** 109-114 (2002).

[12] M. Omar, M. Hassan, and K. Saito, "Optimizing thermography depth probing with a dynamic thermal point spread function", Infared Physics and Technology **46** 506-514 (2005).

[13] O. Breitenstein and F. Altmann, "Inversion of microscopic lock-in thermograms in the presence of emissivity contrast", NDT&E International **39**(8) 636-640 (2006)

[14] M. N. Ozisik, *Heat Conduction, Second Edition*, Wiley-Interscience (1993).

[15] R. C. Gonzalez, Richard Eugene Woods, *Digital Image Processing*, 3rd Edition, Prentice-Hall, New York.

[16] H. Kotera and H. Wang, "Multiscale image sharpening adaptive to edge profile" J. Elec. Imaging **14**(1) 013002 (2005)

[17] J. V. Beck, K. D. Cole, A. Haji-Sheikh, and B. Litkouhi, *Heat Conduction Using Green's Functions*, Taylor & Francis, 1992.

[18] J. Renshaw, S. D. Holland, and R. B. Thompson, "Measurement of crack opening stresses and crack closure stress profiles from heat generation in vibrating cracks", Appl. Phys. Lett **93** 081914 (2008)